ETH
Eidgenössische Technische Hochschule Zürich
Swiss Federal Institute of Technology Zurich

Autonomous Systems Lab
Prof. Roland Siegwart

Bachelor-Thesis

Torque Control of High Compliant Series Elastic Actuator

Spring Term 2010

Supervised by:
Marco Hutter
Mark Höpflinger

Author:
Sebastian Altwegg

Preface

I would like to thank everyone who supported and motivated me during my Bachelor Thesis at the ASL, this includes in particular

- **Prof. Roland Siegwart** for giving me the chance to carry out this thesis at the ASL
- My supervisors **Marco Hutter and Mark Höpflinger**, for their generous support during my project
- **My family and Michèle**, for always motivating me
- **Friends**, for giving me an alternation to my project.

Contents

Abstract

Series elastic actuators (SEA) have been shown to be one of the most appropriate actuation method for legged locomotion. They show a large shock tolerance and introduce additional dynamics, that are useful to achieve a walking or running behavior. In this thesis, a rotary series elastic actuator (RSEA) for torque control of an inverted pendulum has been developed. First the general model of the actuation system gets analyzed and a suitable controller is suggested. Then the physical prototype of a SEA has been realized. The parameters for the spring and actuator have been identified, therefor a comparison between the simulated and the physical model has been made. Finally, the system has been tested with three different torque control modes: zero torque at spring, gravity compensation and virtual spring behavior.

List of Figures

List of Tables

Symbols

Symbols

$\varphi, \Phi(s)$	angle, Laplace transformed angle
γ	gear reduction
Θ	inertia
k_s, d_s	spring constant and damping
T	torque
g	gravity constant
m, l	mass and length of the pendulum
R, L	resistor and inductance of the motor
I, U	motor current and voltage
η	efficiency
κ_i, κ_a	torque and speed constant of the motor
k_p, k_d, k_i	PID gains of the speed controller
$L(s), S(s), T(s)$	Open loop transfer function, Sensitivity and complementary Sensitivity

Indices

spr	spring
mot	motor
gb	gearbox
pen	pendulum
tot	total
des	desired
meas	measured
out	output
z	z axis

Acronyms and Abbreviations

ETH	Eidgenössische Technische Hochschule
ASL	Autonomous Systems Lab
SEA	Series Elastic Actuator
MATLAB	A numerical calculation software by Mathworks

CAD	Computer Aided Design
NX6	A CAD software developed by Siemens PLM Software
LS	Least Square
PID	Proportional, Integrative, Derivative
CPR	Counts per Revolution
RPM	Revolutions per Minute
ITEM	Manufacturer of construction profiles
GUI	Graphical User Interface

Chapter 1

Introduction

1.1 Legged Robots

Legged robots have just started to become popular. Compared to other ground moving robots they have the big advantage of being much more adaptive to difficult terrain. A wheeled vehicle for example may have troubles getting forward on rough and rocky surface whereas the legged robot might be capable of crossing smaller obstacles. A possible field where legged robots might be used is in space exploration. On planets, such as Mars, where nothing is known and the terrain is rather rough they might have a wider range than wheeled vehicles. Further more, legged robots might be used for search and rescue missions. Also for disabled people, who need some sort of walking support, this kind of robot might useful. This all sounds very promising but unfortunately there are at least two fundamental problems in legged locomotion.
The way they move is not at all energy efficient. A lot of effort is put in the swinging of the leg without reusing the negative work for the deceleration of leg. A certain amount of energy gets also lost in the form of collision energy at the end of each swinging movement. Compared to the actuation of legged robots, the driving unit of a wheeled vehicle does not need to accelerate and decelerate continuously for moving.
Another big disadvantage of legged robots is, that they need much more control effort. In a well known environment, controlling the position (kinematic control) of the actuated robot joints might be sufficient. The ALOF robot form the ASL [4] is an example such a kinematic controlled walking robot. However, as soon as the terrain is uncertain, dynamic control has to be applied. Torque control for example could lead to better locomotion performance. To accurately control torques acting an a joint, new actuation approaches are needed. These techniques are summarized in the literature review in Section 1.3.

1.2 Project Outline

The goal of this thesis is to perform accurate torque control by using high-compliant SEA. As an application to evaluate the SEA, a pendulum gets actuated and should be capable of performing different torque control tasks. The pendulum should represent one segment of the leg, the SEA symbolizes the knee or hip joint of the robot.
Torque control is important for legged locomotion in unstructured environment. If only position control is applied, the robot might fail crossing an unperceived obstacle. By applying torque control in each joint of the robot, the overall performance

can be increased and even allows safe human interaction [8].
For accurate torque control, new actuation methods are necessary. A series elastic actuators is accurately torque controllable, lowers the impedance[1] of leg and increases the shock tolerance of the actuator. Since these qualities are desired in legged locomotion, SEAs might be a good actuation method for walking robots.

1.3 Literature Research

1.3.1 Torque Control Problems

Traditionally, the motor torque is regulated by controlling the current at the input of the actuator, based on some information from sensors at the output shaft. To increase the power density (a small actuator that is able to produce large torques) a transmission is used. This however introduces some deleterious effects such as friction and high impedance. The inertia of the motor is seen at the output trough the transmission by the square of the gear reduction. Any collision can cause damage on both, the actuator and the surrounding. To reduce these disadvantages, accurate control and mechanics are needed.

1.3.2 Solutions for Torque Controllable Actuators

There are basically two different techniques for torque controllable actuators: Torque control with a stiff actuator by using sensors at its output and torque control by using series elastic actuators.

- **Stiff actuator with torque sensor**: This method uses a torque sensor that measures the load acting on the joint directly at the output of the actuator. As transducers, most often strain gauges are used. With this torque feedback signal, usually current control at the input of the motor is applied. By using this technique accurate torque control becomes possible. Since the actuator output and the link are still rigidly connected to each other, this method does not significantly lower the impedance and the system is still not shock tolerant. One of the most advanced robot that uses this torque control method is the DLR light weight arm [9] - [11].

- **Series elastic actuator (SEA)**: The actuator in this method is extended by a spring in series to the output of the transmission decoupling the link from the actuator. The effect of the inertia of the motor, seen through the transmission, has therefore no influence on the output. This results in a lower output impedance, higher torque fidelity and improved shock tolerance. For legged locomotion all these properties are desirable. Considering these benefits, SEAs might be a good solution as an actuator for walking robots. Adding a compliance reduces the bandwidth and requires more control effort than a stiff actuator. Different groups ([13], [14]) examined the behavior and the controllability of SEAs and came to the conclusion, that this actuation method is ideal for a lot of applications, for example haptic devices, legged robots or medical rehabilitation devices. This is everywhere where low impedance and high shock tolerance are more important than a high bandwidth [15] - [18].

[1] With impedance is meant, the torque T_{out} at the output that are needed to cause a rotation φ_{out} of the link ($Z(s) = \frac{T_{out}}{\varphi_{out}}$).

1.3.3 Benefits of Springs

There are also other benefits springs might have. R. Alexander [19] suggested, that there are two different ways of saving energy for walking robots by using springs. For losses of kinetic and potential energy, springs might be used to store and release a certain amount of the wasted energy. Another chance of reducing power consumption is when the leg swings with a certain velocity, then at each end of the forward and backward swinging, the energy could be stored and released in springs. He also suggested that spring elements might be used as footpads to increase the shock tolerance of a legged robot.
Animals and humans use the same three benefits of compliance as described in this section. Instead of springs they use tendons of the leg muscles and ligaments the foot to optimize their use of energy.

Chapter 2

General Model

A SEA typically consists of a motor, a gearbox and a spring in series. With a rotational incremental encoder the deflection over the spring is measured and used to control the torque of the motor. The main benefits of such a system are a low output impedance, high torque fidelity and a higher shock tolerance of the actuator. Compared to traditional SEAs, where the controller regulates the current of the motor, two cascaded control loops are used. The outer loop controls the desired torque, whereas the inner loop is responsible for regulating the actuator. G. Wyeth [7] suggested that by having this cascaded structure, and if the motor is seen as a speed source rather than a torque source, the overall performance of the system can be greatly increased. This is the reason why we apply speed control for the inner loop instead of current control.
The model of the system consists of five elements: Torque controller, motor speed controller, motor and gearbox, spring and a mass-pendulum. In the following, the equations of the mechanical model are derived.

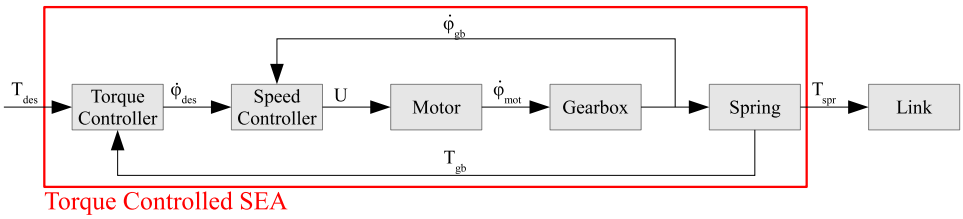

Figure 2.1: Structure overview of the SEA model with the two cascaded control loops and a link at the system output.

Spring: For the spring (Figure 2.2) the simple law of Hook is used. Based on the deflection, the torque acting on the spring is calculated. The deflection is a function of the motor position at the output ($\varphi_{gb} = \gamma \cdot \varphi_{mot}$) and the actual position of the pendulum. A damping term is added to include possible friction. Also important is, that the torques at the input and output of the spring are equal ($T_{spr} = T_{gb}$).

$$T_{spr} = (\varphi_{gb} - \varphi_{out}) \cdot k_s + (\dot{\varphi}_{gb} - \dot{\varphi}_{out}) \cdot d_s \tag{2.1}$$

Motor and Gearbox Mass: The next element that is analyzed is the mass of the motor and transmission (Figure 2.3). Since the output of the transmission is mounted at the other end of the spring, the same torque as before also acts on it.

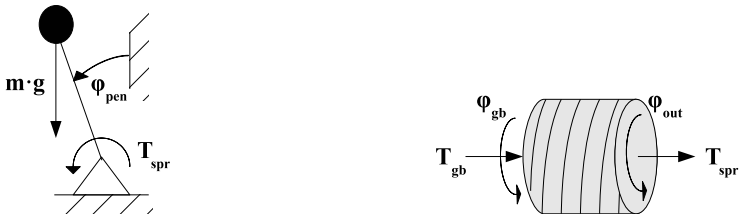

Figure 2.2: The physical representation of the equations of motion belonging to the pendulum and the spring.

On the input we have the torque generated by the motor. The total inertia consists of the mass of the motor and the transmission.

$$\Theta_{tot} = \Theta_{gb} + \Theta_{mot} \tag{2.2}$$

The equation of motion for the total mass is derived by using Newton's second law. The load torque, that counteracts the motor, is nothing else than the spring torque as seen trough the transmission.

$$\Theta_{tot} \cdot \ddot{\varphi}_{mot} = T_{mot} - \gamma \cdot T_{spr} \tag{2.3}$$

Electromagnetic Motor: In addition to the mass, the electrical aspect of the motor has to be considered too. The motor is assumed to be a RL-network with a voltage source and a counteracting back electro magnetic force (Figure 2.3). The torque produced by motors causes the velocity of the mass. This again induces a voltage ($U_{emf} = \kappa_i \cdot \dot{\varphi}_{mot}$) in the RL-network.

$$L \cdot \dot{I} = (U - \kappa_i \cdot \dot{\varphi}_{mot} - R \cdot I) \tag{2.4}$$

The torque that the motor can produce, linearly depends on the current in the circuit.

$$T_{mot} = \kappa_a \cdot I \tag{2.5}$$

Figure 2.3: The general model of the motor: The RL-network belonging to the DC-motor and the equation of motion for the motor and gearbox mass.

Link: The link is assumed to be a pendulum with the inertia Θ_{pend} (Figure 2.2). The equation of motion is influenced by the torque form the output of the gearbox T_{gb} and the gravity, that causes another torque.

$$\Theta_{pen} \cdot \ddot{\varphi}_{pen} = T_{spr} + m \cdot g \cdot l \cdot \sin(\varphi_{pen}) \tag{2.6}$$

It is important to mention that this element is not linear. The link itself is not considered for the controller design and is only used for demonstration reasons. Therefore, the influence of the link is neglected and output position of the spring is assumed to be zero for later analysis.

Chapter 3

Model Analysis

As already mentioned in Chapter 2 the pendulum gets rigidly mounted, since the controller should work independently of the load. This means, its output position is assumed to be zero for all time. With the neglected pendulum influence, we now have a completely linear system and its transfer functions including the two controllers, can be derived. The equations listed in Chapter 2 are Laplace transformed and recombined. The plant of the system consists of the motor velocity controller, the motor, and the spring.
For a first model identification, only the motor control loop is considered. This includes the speed controller, the electrical motor and the motor mass. There is no external torque acting on the motor. The input of this subsystem is the desired velocity $\dot{\varphi}_{des}$ and the output is the measured one $\dot{\varphi}_{mot}$.
A PID controller is used to regulate the speed of the motor. Now it is possible to derive the open-loop transfer function of the motor $L_{mot}(s)$. The complete derivation is done in C.1.

$$L_{mot}(s) = \frac{\dot{\Phi}_{mot}(s)}{\dot{\Phi}_{des}(s)} \tag{3.1}$$

The transfer functions of the motor can now be visualized in a Bode plot, shown in Figure 3.1. The bandwidth of the motor is where the closed-loop transfer function $T_{mot}(s) = L_{mot}(s)/(1 + L_{mot}(s))$ drops below -3dB. For this specific case the bandwidth is around 24.5 rad/s. It is important to mention, that the bandwidth of the complete system has to be below the one of the motor. It would not make any sense to excite the system with higher frequencies than the motor is able to handle. For higher frequencies the actuator-system would act like a low-pass filter.
The derivation of the transfer function for the complete plant is the next step. The goal is to find the relationship between the output torque T_{spr} and the desired input velocity $\dot{\varphi}_{des}$ in $[^\circ/s]$. The back acting torque on the motor mass form the spring gets reintroduced. Since the output of the spring is fixed for all time, this torque is only a function of the motor position and velocity at the output of the gearbox ($\gamma \cdot \varphi_{mot}$ and $\gamma \cdot \dot{\varphi}_{mot}$ respectively). The Laplace transformed equation of the spring is:

$$T_{spr}(s) = \gamma \cdot \Phi_{mot}(s) \cdot (k_s + s \cdot d_s) \tag{3.2}$$

Now, all equations needed for the transfer function $P(s)$ of the plant are derived. In Appendix C.2 the detailed derivation is done.

$$P(s) = \frac{T_{spr}(s)}{\dot{\Phi}_{des}(s)} \tag{3.3}$$

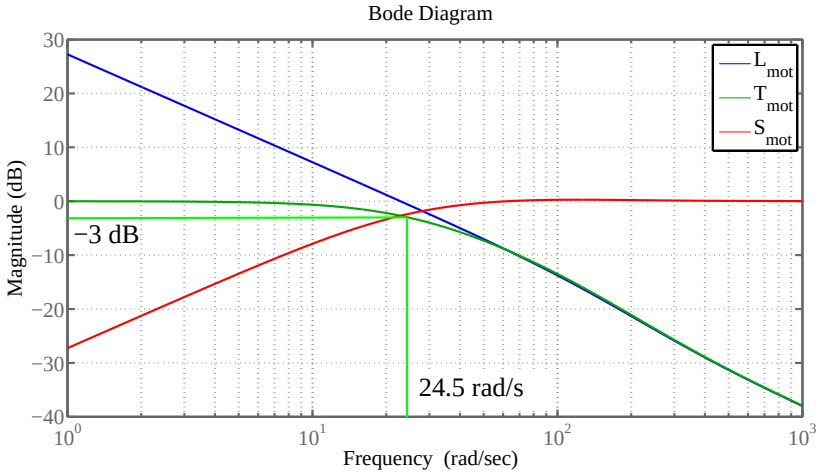

Figure 3.1: Bode plots of the inner loop belonging to the motor, gearbox and speed controller. It shows the open- ($L_{mot}(j\omega)$) and closed-loop ($T_{mot}(j\omega)$) transfer function, as well as the sensitivity $S_{mot}(j\omega)$ of the motor system.

3.1 Torque Controller for the General Model

Since the model is known, first controller gains can be found by loop-shaping such that the overall bandwidth is below the bandwidth of the motor. It is desirable, that there is no steady state error. The open-loop transfer function of the plant P(s) has a pole a $s = 0$. Therefore, the plant of the SEA with the fixed pendulum contains an open integrator and a P-controller can be used to satisfy the required zero steady state error behavior. The combination of the controller and the plant P(s) of the system leads to the open-loop transfer function $L_o(s)$ shown in equation 3.4. It takes a desired torque T_{des} at the input and returns the torque action on the spring T_{spr}. In Figure 3.2 the Bode plot of the system is shown. The bandwidth of the system, as well as the maximum sensitivity $S_{o,max}(j\omega)$ and the maximum complementary sensitivity $T_{o,max}(j\omega)$ are calculated and summarized in Table 3.1.

$$L_o(s) = \frac{T_{spr}(s)}{T_{des}(s)} \tag{3.4}$$

To check the stability of the system, the Nyquist theorem is used. The open-loop transfer function $L_o(s)$ has one pole in the origin and all others have negative real part. Following the Nyquist stability criteria [3], the number of encirclements of the point -1 by $L_o(j\omega)$ should be $\frac{1}{2}$. As in Figure 3.3 can be seen, this is the case. There are also no zeros with a positive real part in the open-loop transfer function. Therefore, the plant with a P-controller is stable and minimum phase.

Table 3.1: Bandwidth, $S_{o,max}(j\omega)$ and $T_{o,max}(j\omega)$ of the SEA

Characteristic	Unit	Identified value
Bandwidth	[rad/s]	17
Maximum sensitivity, $S_{o,max}(j\omega)$	[-]	1.23
Maximum complementary sensitivity, $T_{o,max}(j\omega)$	[-]	1

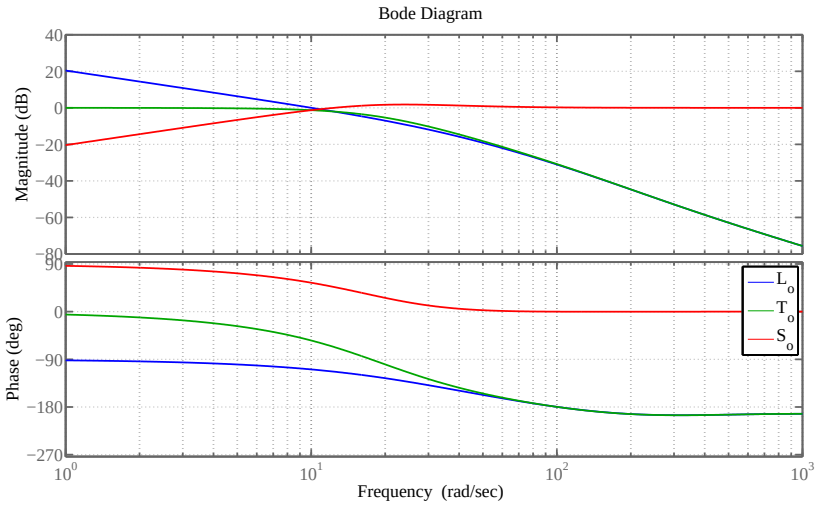

Figure 3.2: Bode plots belonging to the outer control loop of the complete system. It includes the open- ($L_o(j\omega)$) and closed-loop ($T_o(j\omega)$) transfer function, as well as the sensitivity $S_o(j\omega)$.

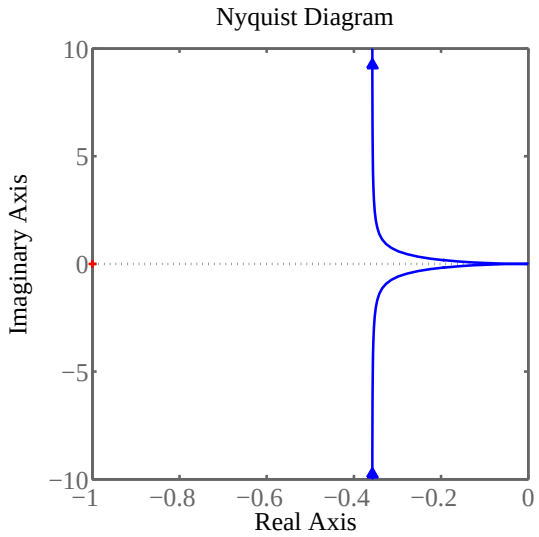

Figure 3.3: Nyquist plot of the open-loop transfer function $L_o(s)$ of the complete system.

After the analysis in the frequency domain, the result can be shown in the time domain. Therefore step response of the system is shown in Figure 3.4.

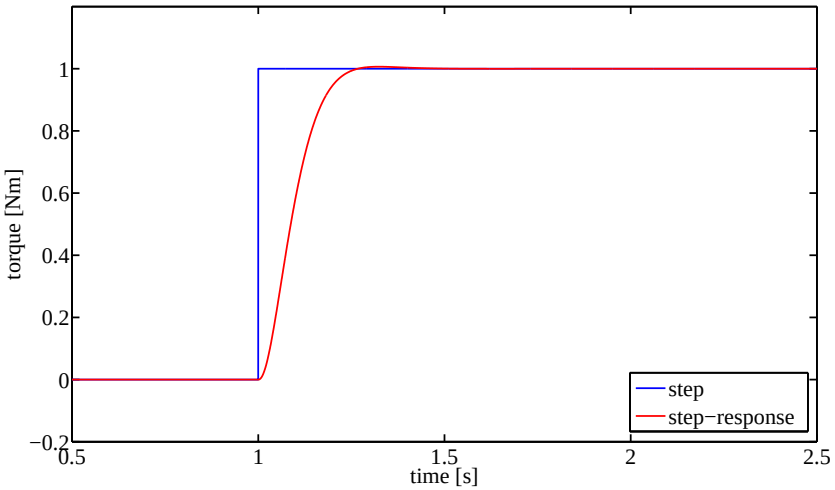

Figure 3.4: Step response of the system with a fixed pendulum by using a simple P-controller.

To see how the system behaves in the free pendulum mode a graphical visualization of this element is implemented additionally. With a P-controller used for the fixed pendulum, simulations have shown, that the controller is too slow to perform the demanded torque. An integrating part solves this problem and shows, that the free pendulum is able to perform torque control tasks such as gravity compensation, virtual spring behavior and zero torque at the actuator output.

Chapter 4

Physical Prototype

A traditional SEA consists of a controller, an actuator with gearbox and spring in series. For our SEA we use a cascaded control loop that consists of an inner loop with a motor velocity controller and an outer loop that regulates the demanded torques. At the output of the SEA a pendulum is mounted as representation of a leg segment. The actuator and spring itself should represent the hip or knee actuation of a legged robot. It is important to mention that the SEA should work, independently of what kind of load is attached. The conclusion out of this is, that the controller is not model based. The pendulum is only used for demonstration reasons. The following list provides an overview of the elements used in the SEA prototype.

- Incremental encoder to measure the spring deflection (1)[1]
- Torsional spring (2)[2] and spring-coupling (3)
- Motor-shaft coupling (4)[3]
- Actuator (6) with gearbox (5) and motor position encoder (7)[4]
- Motor speed/current controller
- Torque controller
- Pendulum

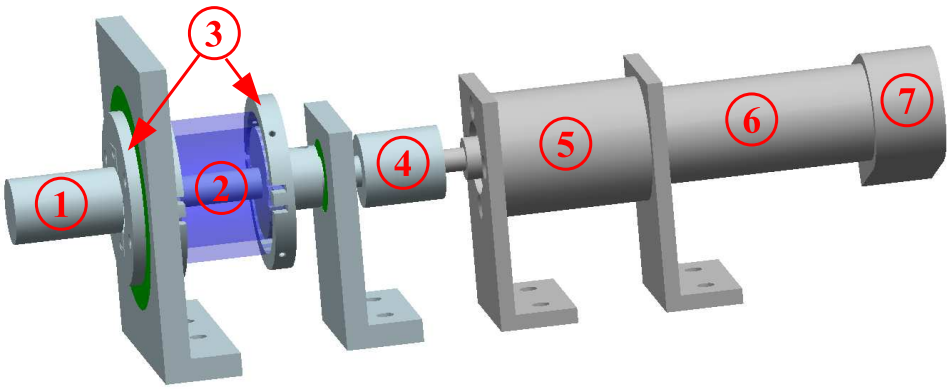

Figure 4.1: CAD model of the SEA, including the an rotational incremental encoder (1), the spring (2) and its coupling (3) and the motor (6) with transmission (5) which is connected to the shaft with another coupling (4).

[1] Avago incremental encoder AEDA-3300
[2] Heli-Cal machined torsional spring
[3] Mädler self-aligning couplings
[4] Maxon motors

4.1 Actuator and Speed/Current Controller

The complete actuation system including the motor controller is produced by Maxon. Choosing the right actuator depends on the application, the torques as well as on the speeds that have to be provided. For our application a relatively small actuator with a high maximum speed in combination with a gearbox is used. This allows the actuator to operate at his "sweet spot", at high speed and low torque, where the output can provide high torques at lower speed.
The motor controller (EPOS) regulates the motor voltage depending on the desired and measured speed or current respectively. The data for the chosen actuator system can be found in Appendix B.

4.2 Torsional Spring and Coupling

The choice of the spring constant is based on previous work on a hopping leg prototype [1]. The torsional spring was manufactured by the company Heli-Cal. For the given spring, a suitable coupling had to be designed. The considerations and applied solution for each requirement are listed below.

- **Precision**: This is the most important requirement of the coupling design. It is necessary, that there is no backlash that origins in the spring and coupling when the actuator rotates. There were already two slots on both sides of the spring (b). Two bars (a) in each half of the coupling fit together with the slots in the spring and therefore hinder it form slipping. The bar and the slot of the spring is shown in Figure 4.4 The spring is lowered in a circular slot in both halves. This circular slot (c) is shown in Figure 4.4
- **Sensor placement**: The given encoder had to be integrated in the system to measure the absolute deflection over the spring. This is necessary to achieve accurate torque control. A good location for the sensor turned out to be at the outer coupling (3o). The incremental encoder measures the revolutions of the shaft which is fixed with a locking pin (d) at the inner half (3i) of the coupling. The axle can freely rotate in a bearing, placed in the outer half of the coupling (3o). Since the encoder is mounted there it measures the absolute deflection over the spring. Therefore, the backlash that origins in the motor and gearbox, has no influence on the measured deflection values.
- **Pendulum**: For the pendulum four screw holes were made in the outer coupling, where different possible versions of pendulums can be mounted.
- **Base, modularity**: The last requirement that has to be satisfied is, that the complete installation has to be mounted somehow. This is done with two carriers that include ball bearings, where the shaft and the outer coupling half are placed. Another issue that has to be considered is the modularity of the construction.

In Figure 4.2 the outer coupling half are illustrated. The shaft, that connects the both halves of the coupling, is shown in Figure 4.3. Also shown is the modularity view of the spring coupling in Figure 4.4. They all have been designed in the NX6 CAD software.

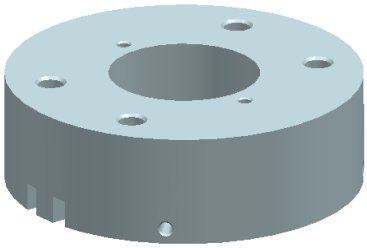

Figure 4.2: The outer half (3o) of the coupling, constructed in the NX6 CAD software. The screw holes are for mounting the encoder and the link.

Figure 4.3: The shaft of the coupling constructed in a CAD software. The left tip is for causing a revolution in the incremental encoder. Also visible the cut-in slot for the locking clip.

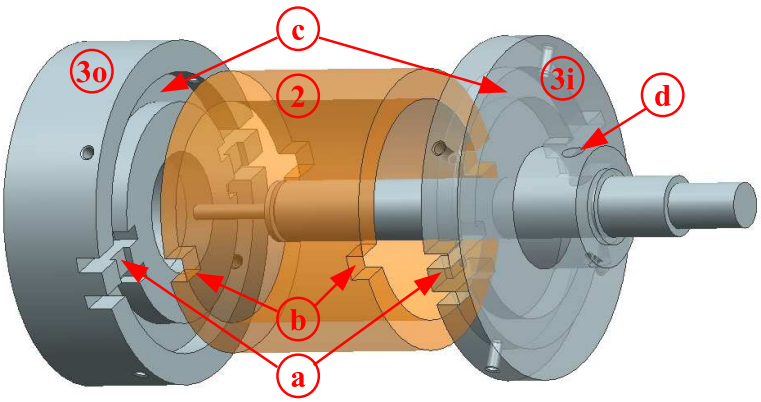

Figure 4.4: Modular view of the spring coupling with the outer (3o) and the inner (3i) half of the coupling and the spring (2) in between.

4.3 Sensor

There are different ways of measuring the deflection over a spring but since we have to deal with a torsional spring, a rotary encoder (Figure 4.1 (1)) seems to be a reasonable solution. The company Avago sells incremental encoders with different resolutions. For our prototype a resolution of 20'000 counts and after quadrature encoding 80'000 counts per revolution is chosen. This results in, that even a very small deflection over the spring is detected. The technical data of the "Avago AEDA-3300 TE1 Incremental Kit Encoder Top-Down Version" can be found in Appendix B.
The position and velocity of the motor is sensed by a transducer that is attached at the opposite of the actuators output (Figure 4.1 (7)). This encoder has a resolution 500 counts per revolution. Again, after quadrature encoding this turns into 2000 counts per revolution.

4.4 Pendulum

The main criteria is, that the pendulum should be robust and rigidly connectible to the outer coupling half. Therefore, a rectangle profile is used for the pendulum. The dimensions of the link have been chosen such that its inertia corresponds to a leg segment of the hopping leg prototype.

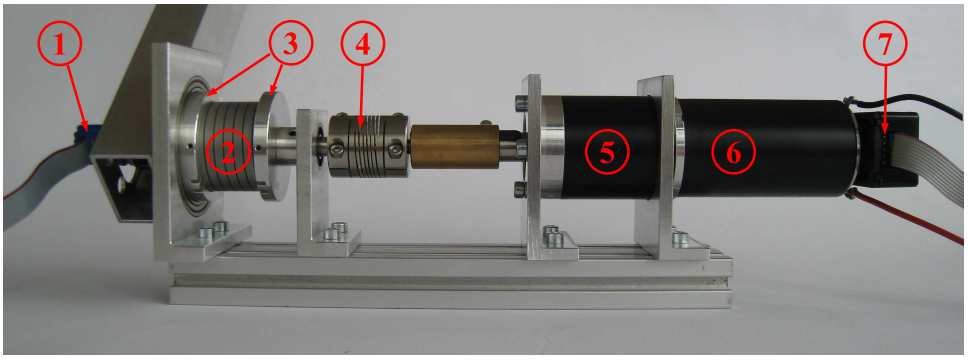

Figure 4.5: The final version of our SEA prototype consisting of (from left): Encoder, pendulum, coupling and spring, actuator-shaft coupling, motor and transmission and the encoder of the motor.

Chapter 5

Model Identification

Since accurate modeling is the basis for successful controller design, it is necessary to compare the model of the system designed in MATLAB Simulink and the actual physical prototype. The verification and identification process is separated in three steps listed below:

1. The motor with gearbox and its controller in Section 5.1.
2. Characteristics of the spring in Section 5.2.
3. Complete system with a simple P-controller in Section 5.3.

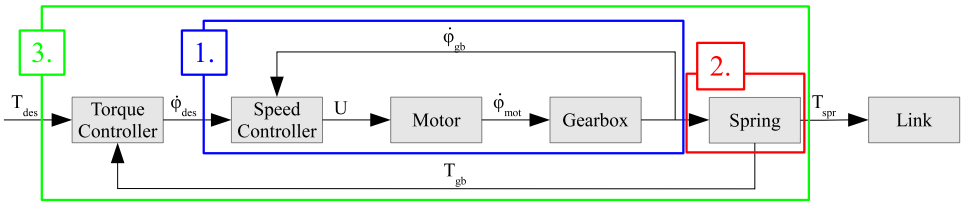

Figure 5.1: Overview of the three model identification steps.

In each step, the uncertain or unknown parameters have to be identified and the model needs to be verified, by comparing it with the physical system. In Table 5.1 the parameters from each loop that need to be identified are listed.

Table 5.1: Parameters that have to be identified, separated in the three identification steps.

Identification step	Parameter	Symbol
Motor loop	EPOS controller parameters	k_p, k_i, k_d
Spring	Spring characteristics, motor elasticity	k_s, k_{mot}
	gearbox efficiency	η_{gb}
Complete System	Torque controller parameter	K_p

5.1 Motor and Speed Controller

The actuator consists of the electrical and the mechanical part with the mass. The parameters belonging to this motor and the gearbox are provided by Maxon Motors and can be found in Appendix B. The controller parameters for the EPOS speed controller are not known and need to be identified.
To identify these controller parameters and to verify the model of the motor loop, the system is excited with a step. Independently of the demand speed, the simulated step-response coincide very much with the response of the actual subsystem. The small difference between the simulated and measured data probably origins in the model of the EPOS. The EPOS control parameters are only an estimation and do not exactly coincide with the physical EPOS. In Figure 5.2 a step response of a 5 rad/s demand velocity is shown.
Another state that might help to identify the parameters, is the motor current. The same parameters and Simulink model as before are used and the measured and simulated values of the current are again plotted vs. the time. The plot shows, that there is more current needed in the physical system than in the simulation. A possible interpretation for this phenomenon is, that a breakaway torque forces the motor to put more effort in the acceleration of the mass. This effect is not considered in the Simulink model. The effect, that we have negative values for the current after the step is due to controller offsets in the EPOS current control implementation[1]. The current vs. time plot is shown in Figure 5.3.
In Table 5.2 the identified values of the controller parameters are listed.

Table 5.2: Motor loop: Parameter identification of the EPOS controller gains.

Parameter	Provided value	Identified value
k_p	-	0.0039
k_i	-	0.95
k_d	-	0

The results of this identification step leads to the assumption, that the Simulink model of the motor loop can be used for further analysis. Also the identified controller parameters show a reasonable behavior, compared to the physical motor speed controller. The small differences between the measured and the simulated data could be explained with the not exactly known EPOS controller parameters and with additionally needed breakaway torque in the physical motor.

[1] Personal communication with the Maxon support center

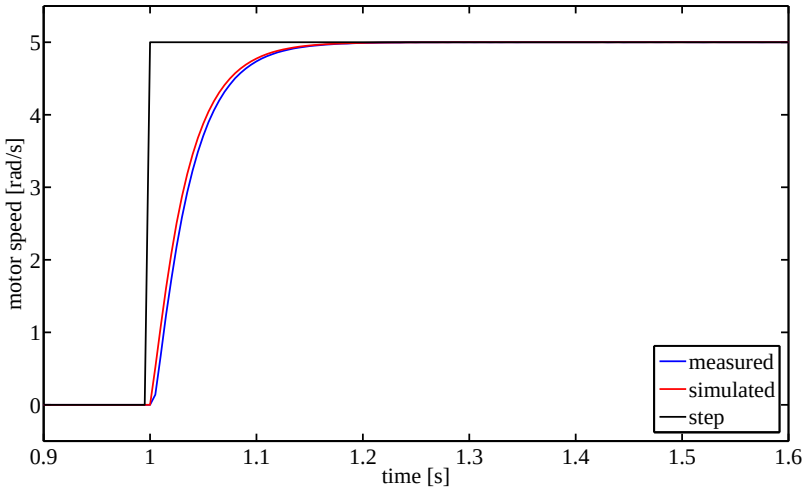

Figure 5.2: Motor identification with a step response of a speed demand of 5 rad/s. The simulated and the measured data coincide well, the slight error is due to not exact EPOS values for the simulation.

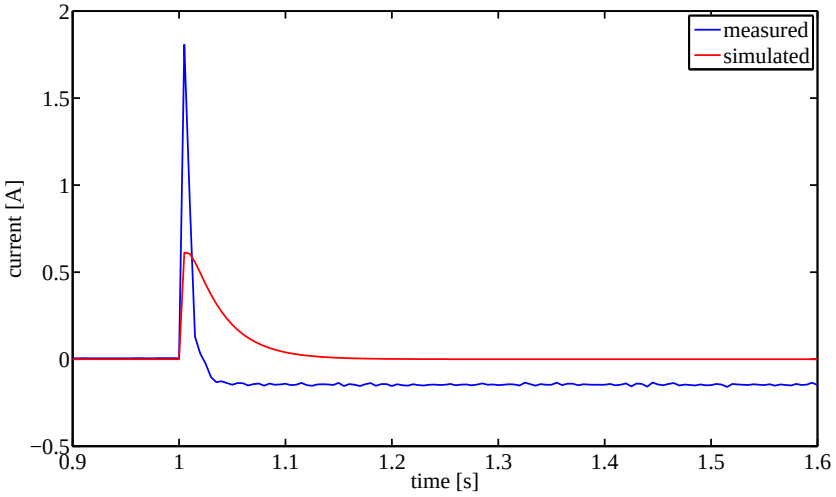

Figure 5.3: Motor current vs. time for the identification of the motor, gearbox and speed controller. The negative current after the peak is an error in the EPOS of Maxon.

5.2 Spring

5.2.1 Spring of the Hopping Leg Prototype

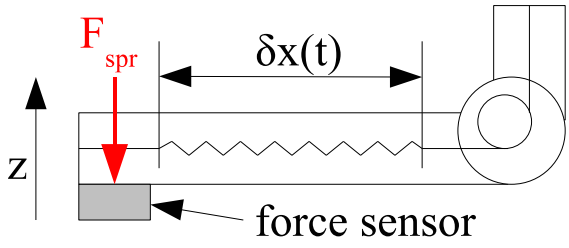

Figure 5.4: The test bench of the hopping leg prototype: The sensor measures the forces acting on the linear spring, placed inside the leg. An encoder mounted in the knee joint is responsible for measuring the deflection.

As a preparation to the parameter identification of the spring, the existing leg developed by M. Hutter [1] is used and the characteristics of the spring in its knee are derived. The same procedure is later used to derive the behavior of the spring in the rotary series elastic actuator. For the identification, a force sensor is placed at the end of the link. The system is positioned and fixed such that nothing else can move than the knee joint. In Figure 5.4 the test bench is illustrated. The relevant signals that we get are the position of the motor and encoder, the motor current and the force in z direction. The spring has been mounted with a certain pre-compressing force which has to be considered later when the characteristic is calculated with a least squares method (LS-method). Furthermore it is assumed that the spring behavior is linear. Following these assumptions, the general equation of the spring results in:

$$F_{spr} = k_s \cdot \delta x(t) + F_0 \tag{5.1}$$

The parameters that have to be derived are the spring constant k_s and the pre-compressing force F_0. The total force acting on the spring, is proportional to the spring deflection $\delta x(t)$. F_0 is necessary to include the pre-load that is acting on the spring[2]. By using the LS-method, these parameters are getting calculated such that the square of the resulting error form the measured data is minimal.

$$\pi = \begin{pmatrix} k_s \\ F_0 \end{pmatrix} \qquad \tilde{y} = \begin{pmatrix} F_z(1) \\ F_z(2) \\ \vdots \end{pmatrix} \tag{5.2}$$

$$H = \begin{pmatrix} \delta x(1) & 1 \\ \delta x(2) & 1 \\ \vdots & \vdots \end{pmatrix} \qquad W = \begin{pmatrix} 1 & 0 & \\ 0 & 1 & \\ & & \ddots \end{pmatrix} \tag{5.3}$$

With these definitions in place, we now can find the parameters k_s and F_0. The solution to the LS-problem is the following equation [2].

$$\pi = \left[H^T \cdot W \cdot H\right]^{-1} \cdot H^T \cdot W \cdot \tilde{y} \tag{5.4}$$

[2]To avoid, that the torque form the pre-load does not effect our LS-method, the first and last 200 measurements (around zero deflection) are not included in the LS procedure.

In Figure 5.5 the results of one experiment are shown. The blue curve is the measured force transformed into torque. By using the results of the above described LS-method, the optimal solution to the measured data is added to the plot as the red line. In green the torque calculated by the deflection, using the parameters found in the LS-optimization, is indicated.
The step in Figure 5.5 near zero deflection is due to the pre-load already acting on the spring. What clearly is visible, that the curves diverge at low and high deflection. This hysteresis error might be due to friction effects in the gearbox and the motor. The conclusion of this identification step is, that torque control can only be applied for large deflections. There the behavior of the spring is more or less linear.
It is important to mention, that in this leg prototype a linear spring is used and the deflection is caused by a transmission that transforms rotary to a linear movement. All the data used for the plots are converted into rotary movements. Also the linear spring is mathematically transformed to a rotary spring. Furthermore the spring is mounted inside the leg such that there is more friction compared to my rotary series elastic actuator.
The results of the identification process are shown in Table 5.3. By taking the mean value of five experiments, the spring constant is calculated. The difference of the provided and measured value can be explained by the not exactly known position of the force sensor.

Table 5.3: Comparison of the measured and provided values of the linear spring constant used in the hopping leg prototype

Spring constant from	k_s [Nm/mm]
Provided Value	6.1
LS-method	6.22

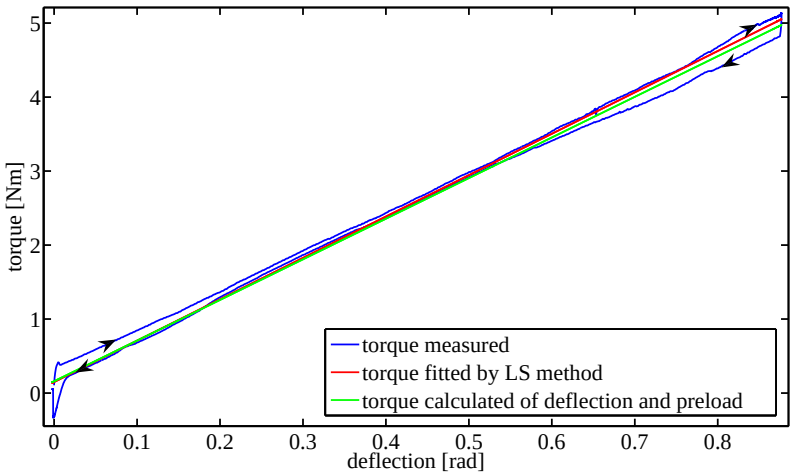

Figure 5.5: Torque vs. deflection of the spring in the prototype hopping leg. A linear behavior of the spring with slight hysteresis error and an already acting pre-stressing torque.

5.2.2 Spring of the Rotary SEA

The next element that has to get verified is the spring of the SEA. Due to the technical drawing of the spring, provided by the producer Helical, it is assumed that the elastic coupling has a spring constant of 6.22 $\frac{Nm}{rad}$. The test bench of the identification experiment is shown in Figure 5.6.

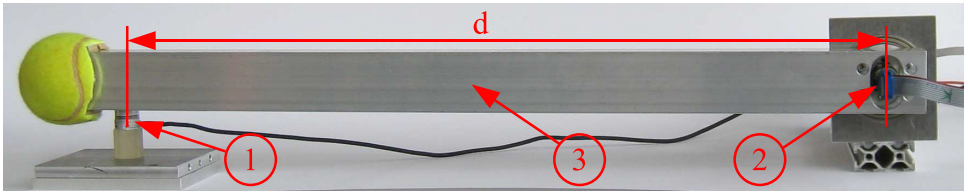

Figure 5.6: The test bench of the inverted pendulum (3) and the series elastic actuator. The load cell (1) measures the forces, the incremental encoder (2) the deflection over the spring.

The pendulum is placed on the force sensor and a counter clockwise revolution of the motor causes a torque on the spring. With this constellation, the output of the spring cannot move and is therefore assumed to be zero. With a force sensor, placed at a distance d form the joint, the applied force is measured. By using Hook's law this lead us to the following equation for the relationship between the measured force F_{meas}, the measured deflection φ_{spr} and the torque T_{spr} acting on the spring.

$$F_{meas} \cdot d = \varphi_{spr} \cdot k_s = T_{spr} \tag{5.5}$$

The system is excited with a step for desired motor position. Although the signal of the encoder is very linear and clean, the spring constant is calculated by using the same LS-method as before. In Figure 5.7 the result is shown. The rotary spring used in this SEA can be seen as perfectly linear torque element. The mean value for the calculated spring characteristics k_s of five measurements is compared in Table 5.4 with the values provided by Heli-Cal.

Table 5.4: Comparison of the measured and provided values of the torsional spring constant used in the SEA

Spring constant from	k_s [Nm/rad]
Technical drawing	6.22
LS-method	6.23

This leads us to the assumption that the given values are correct. The slight deviation can be explained by the position of the force sensor: If the value d for the distance of the force sensor is not exact, the calculated torque differs form the actually acting torque. For further analysis it can be assumed, that the spring acts as an ideal torque element with no hysteresis error.

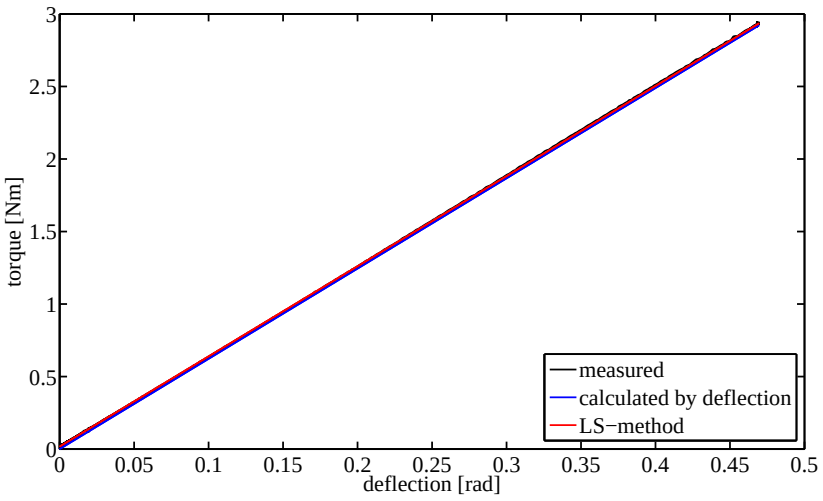

Figure 5.7: Spring parameter identification: Torque acting on the spring depending on the deflection for a motor demand position of 0.5 rad. This leads to the characteristic of the spring which turns out to be a perfectly linear torque element.

Due to the fact, that the output of the spring is fixed and therefore should not move, the deflection measured over the spring corresponds to the motor output position. However, as can be seen in Figure 5.8, the deflection of the spring does not coincide with the motor position. The position sensor of the motor and the incremental encoder are both tested separately and they seemed to work fine, so the source of this effect is not an encoder. It seems that the difference between both measurements is linear. One reasonable explanation for this phenomenon is that the motor, the gearbox and the bar of the pendulum itself have a certain flexibility. The position of the motor is always a factor 1.069 too large compared to the encoder position. Based on these measurements the "spring constant" of the motor k_{mot} can be derived.

$$k_{mot} \cdot (\varphi_{mot} - \varphi_{spr}) = T_{spr} = k_s \cdot \varphi_{spr} \tag{5.6}$$

This equation is now solved for k_{mot} leads us to the elasticity of the motor.

$$k_{mot} = k_s \frac{\varphi_{spr}}{\varphi_{mot} - \varphi_{spr}} \tag{5.7}$$

For the actuator of the SEA, this corresponds to a k_{mot} of 79 [Nm/rad]. All the results for the motor position and velocity could now be corrected for precise analysis of the complete system. However, this is not necessary because we want to do torque control and by measuring the absolute deflection over the spring, we get the exact value of the torque acting on the joint. The flexibility of the actuator does not have any influence on that. Simply for calculations that include motor position or velocity this effect has to be included.
The torque acting on the spring can also be verified by measuring the current the actuator needs to provide the demanded torque. The torque constant of the motor is provided by Maxon. It is important to include the gearbox efficiency in the calculations of the torque and to consider that the torque flow changes between winding the spring up and decreasing the spring deflection back to zero. Therefore, the winding up process has to be multiplied by the efficiency whereas the opposite process has to be divided by the efficiency. For the extending process of the spring, the current-calculated torque coincides with the optimal solution. The reverse process did not share this quality. This might be due to different efficiencies depending on the direction of the actuator rotation. Therefore, the efficiency of the reverse process (relaxing of the spring) is corrected and leads to the result shown in Figure 5.9. A possible influence on the reduced efficiency might be the age and health condition of the gearbox and the motor.
The parameters identified in this section are summarized in Table 5.5.

Table 5.5: Identified parameters for the spring characteristics, the gearbox efficiency and the elasticity of the motor.

Parameter	Unit	Provided value	Identified value
Spring constant, k_s	[Nm/rad]	6.22	6.23
Motor elasticity, k_{mot}	[Nm/rad]	-	79
Gearbox eff. extending, η_{gb1}	[-]	0.7	0.7
Gearbox eff. relaxing, η_{gb2}	[-]	0.7	0.63

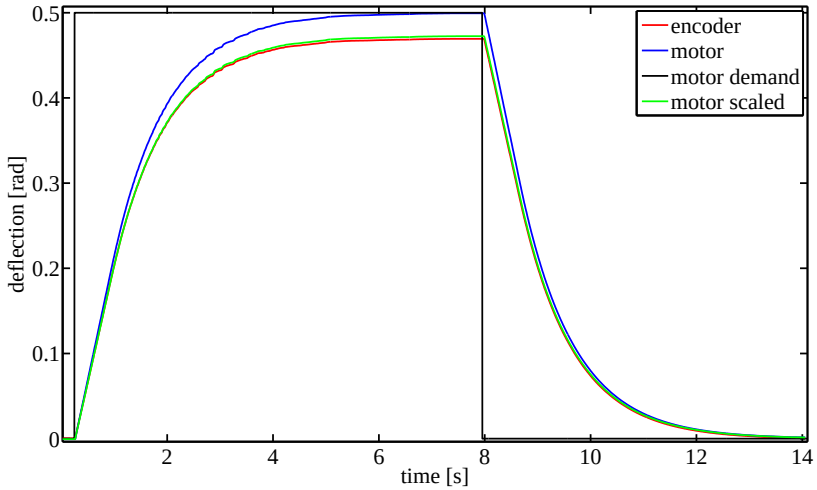

Figure 5.8: Motor elasticity identification: Step responses for a demand motor position of 0.5 rad. Also included is the scaled motor position by including its elasticity.

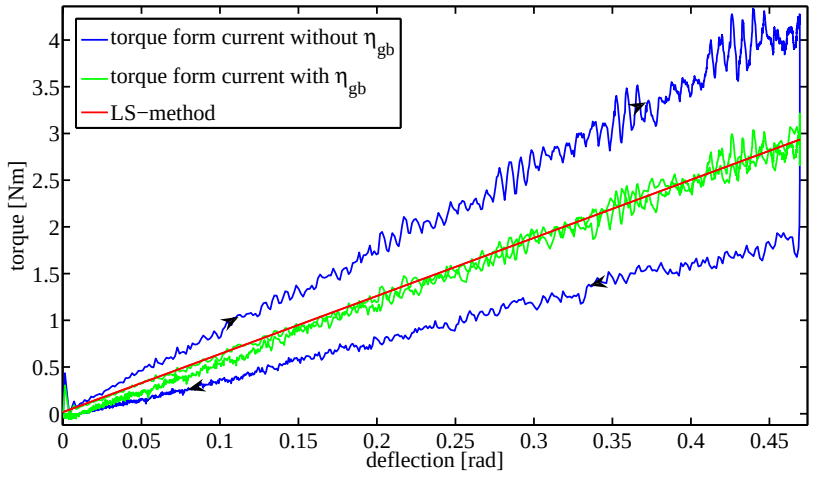

Figure 5.9: Gearbox efficiency identification: Torque acting in the spring calculated of the motor current. The efficiency η_{gb} has been modified such that they coincide with the actual torque.

5.3 Complete System

The last step of the identification process includes the complete system. The same configuration as in Section 5.2 is used, but this time the system is excited by a demand torque step instead of a demand position. A simple proportional torque controller is used. For the simulation and the controller of our prototype, the same P-controller gain K_p is chosen. The torque is calculated with the deflection and the measured force, then the two results are compared. If they coincide it can be assumed that the complete prototype behaves like the simulated system and that the P-controller gain is the same as used for the physical prototype. In Figure 5.10 the torques, by using different calculation schemes, are plotted. One torque is measured and transformed with the force sensor, the second one is the simulated version and the last one is calculated based on the deflection. They all coincide very much and therefore, it can be assumed, that the torque calculated of the deflection is the actually acting torque on the spring. This also shows that the Simulink model has the same behavior as the physical prototype.
It is also interesting to look at the torque, calculated with the motor current, shown in Figure 5.11. In the deflection process the current does not continuously increase. Just after the start the current decreases for a short time and the increases again. By varying the integrator gain of the EPOS speed controller in the model, this peak changes its shape. This leads to the assumption that this effect depends on the control parameters of the EPOS speed controller. Since the same effect occurs at the measured data, it can be assumed that physical EPOS has a similar behavior. The effect, that the measured current is larger at the beginning, could again depend on the breakaway torque.

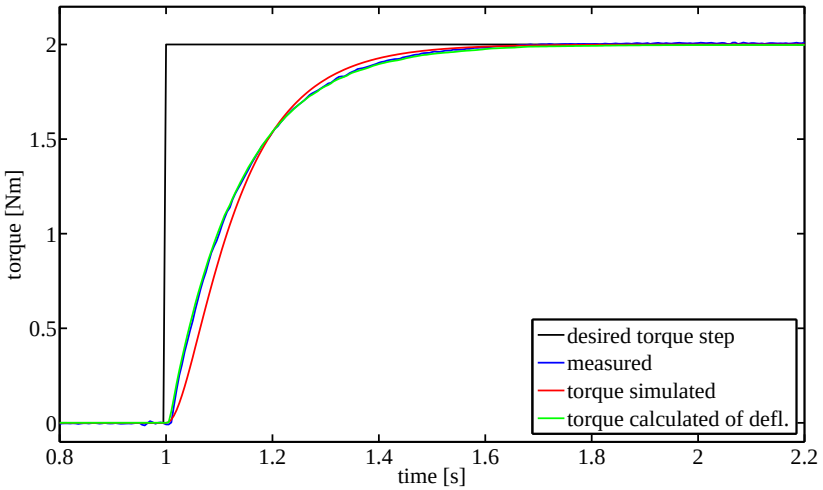

Figure 5.10: Different calculation schemes for a torque step response: The measured data form the load cell, the torque calculated on behalf of the spring deflection and simulated data are shown.

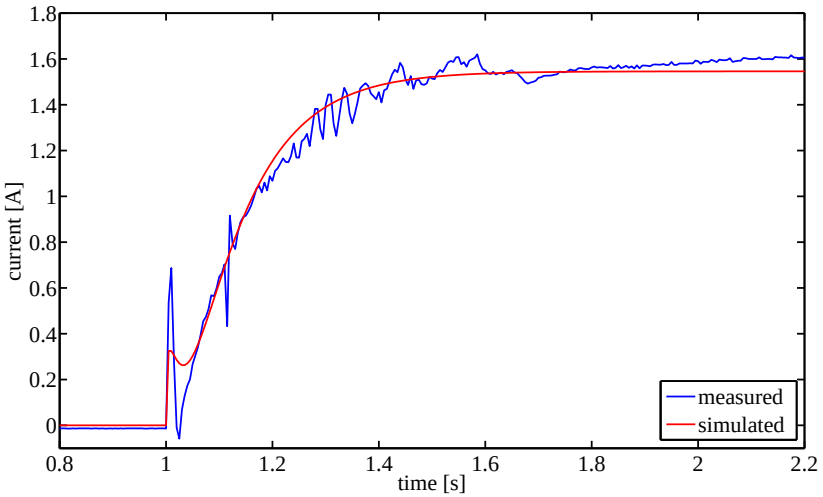

Figure 5.11: Current of the motor for a demand torque step of 2 Nm. The measured and simulated data share the same step response behavior.

Chapter 6

Controller Implementation

The torque control structure of the SEA consists of two cascaded control loops. The inner loop controls the speed of the actuator, the outer loop is responsible for controlling the torques acting at the output of the SEA. The complete control structure is shown in Figure 6.1.
The torque controller is implemented on the National Instruments sbRIO[1] (Single-Board RIO). This is a device, that includes a RT (micro processor) and a FPGA (Field Programmable Gait Array). Different I/O (input/output) modules can be connected to the sbRIO. In the case of this SEA the I/O modules are a differential digital input module[2], that gets data form the incremental encoder and a CAN module[3], that communicates with the EPOS (motor controller). Depending on the behavior mode (Section 6.1-6.3) the desired torque is calculated on the RT with a frequency of 200 Hz and then sent to the FPGA.
On the FPGA the actual torque controller is implemented. It takes the measured deflection and calculated the torque acting on the spring. The FPGA works with a frequency of 40 MHz. Considering that the resolution of the incremental encoder is 80000 counts per revolution, this is necessary. Depending on the measured and desired torque, the desired motor velocity is controlled. The FPGA communicates with the EPOS with a frequency of 1 kHz.

$$\dot{\varphi}_{des} = f(T_{des}, T_{meas}) \tag{6.1}$$

The motor gets controlled by a Maxon position controller (EPOS) [5]. A desired motor speed in [rpm] is calculated on the sbRIO and then sent to the EPOS. There the motor voltage is controlled depending on the desired and measured motor speed.

$$U = f(\dot{\varphi}_{des}, \dot{\varphi}_{mot}) \tag{6.2}$$

This motor controller operates with a frequency of 1 kHz. The internal control structure is already implemented on the EPOS. An identification of its control parameters is done in Section 5.1.
The behavior of the spring, having one end fixed, with a simple P-controller is shown to be stable and accurate. Since the fixed system is linear and there is no static error, a P-controller is sufficient. At low proportional gains the system does not overshoot and reaches smoothly the demanded torque. Increasing the P gain leads to an overshooting system. In Chapter 5 such a controller was used to verify the system.

[1] Single-Board RIO: NI sbRIO-9601
[2] Differential digital input module NI 9411
[3] CAN module NI 9853

However, first experiments with the free pendulum have shown, that the P-controller developed in Simulink is not sufficient for several torque control tasks. An integration part improves the overall performance greatly. The corresponding I-gain is found by manually tuning the parameter, such that the system does not overshoot to much and that there is no long oscillating after having reached the desired torque. This PI-controller gets tested in the next sections.

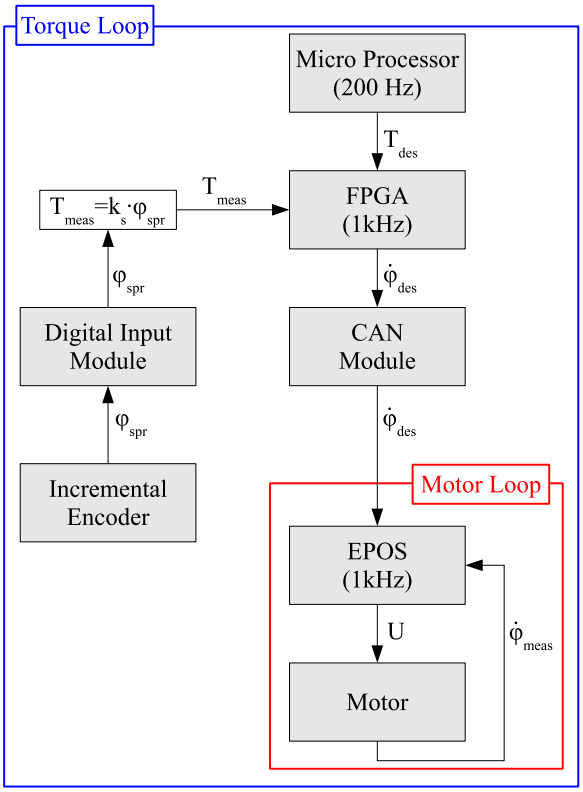

Figure 6.1: Control structure for the SEA with cascaded control loops: the inner loop controls the motor velocity, the outer loop controls the desired torque.

6.1 Gravity Compensation

The demand torque for this control mode depends on the actual pendulum position φ_{pen}, the mass m, and the length l of the pendulum.

$$T_{des} = m \cdot g \cdot l \cdot \sin(\varphi_{pen}) \tag{6.3}$$

In Figure 6.2 the desired and measured torques are plotted vs. the time. Besides the peaks at the beginning and the end of each change of the position the controller works very accurate. The reason for the peaks is, that the controller and the actuator are not fast enough to react to the changing demand torque. When accelerating the pendulum, the spring experiences an additional deflection before the actuator is providing the desired torque (second peak at each horizontal line). Also when stopping the moving pendulum, the actuator still moves for a short time and the spring experiences again an additional deflection (first peak at each horizontal line).

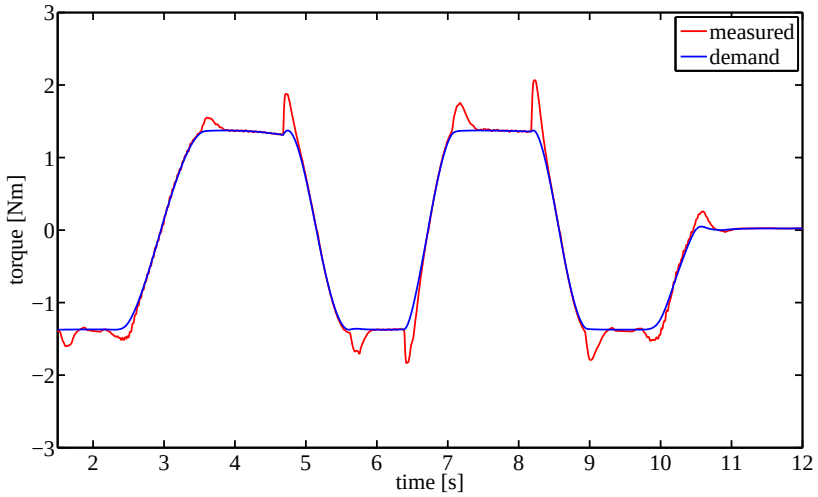

Figure 6.2: Gravity compensation torque control mode applied on the physical prototype. The measured and demanded torques have high coincidence.

6.2 Virtual Spring Element

For this mode a virtual spring behavior gets implemented. The desired torque is calculated by using the deflection over the physical spring and the desired virtual spring stiffness k_{virt}.

$$T_{des} = k_{virt} \cdot \varphi_{spr} \tag{6.4}$$

The measured torque follows the demanded value almost exactly. The fact that the maximum torque at each swinging is not reached, leads to a damping of the system what clearly can be seen in the Figure 6.3. This figure should represent the behavior of a spring with a spring stiffness of 4 Nm/rad.

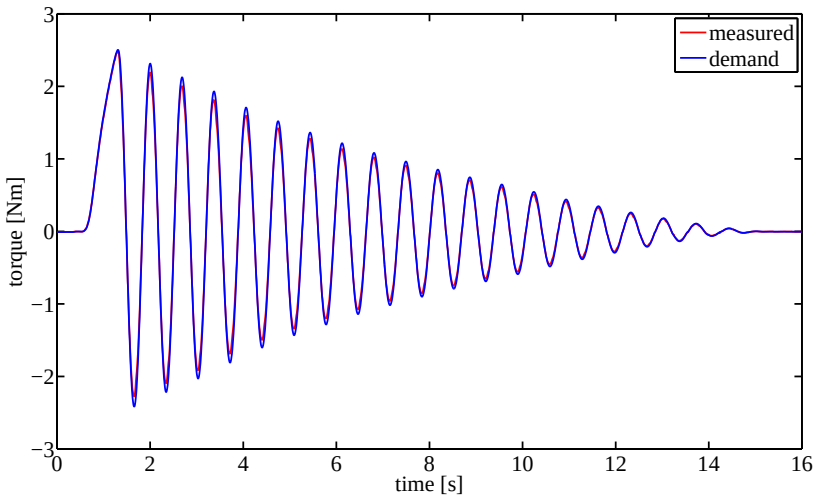

Figure 6.3: The torque acting on the pendulum for a demanded spring constant of 4 Nm/rad compared with the demand torque calculated by the LabView software.

What is interesting to mention, is that for a spring constant of over 6.223 (this is the characteristic of the SEA spring) the pendulum does not get damped any more, it becomes unstable and the amplitude goes to “infinity”.

6.3 Zero Torque on Spring

The "zero torque on the spring" torque control task is the most difficult one and shows the worst result of all three torque control modes.

$$T_{des} = 0 \tag{6.5}$$

The reason for the bad behavior might be again the too slow controller. Instead of swinging "infinitely" the slow controller damps the pendulum. By increasing the controller gains this problem might get solved. However, by doing this, the system is not anymore actuated smoothly and begins to oscillate.

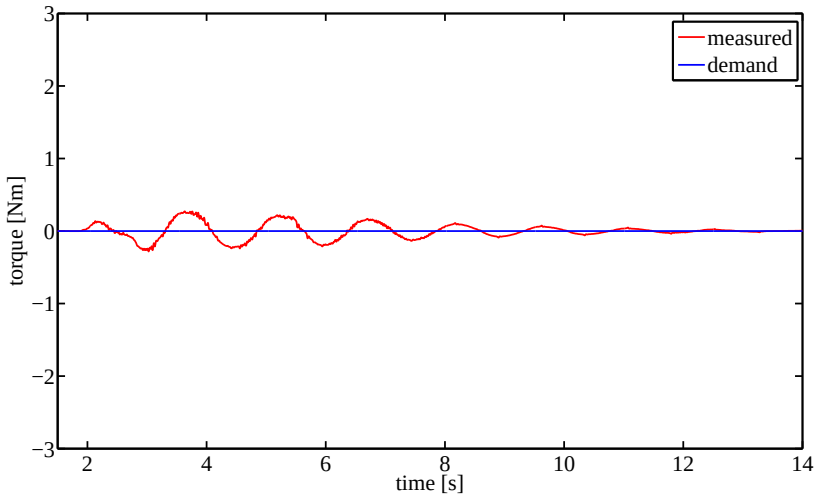

Figure 6.4: The "zero torque at the spring" torque control mode shows the worst result of the applied control modes. This is due to the fact that the sytem is too slow.

Chapter 7

Summary and Contributions

7.1 Result Summary

In this Bachelor Thesis a series elastic actuator for accurate torque control has been developed. This includes the following steps and results:

- **Hardware**: A physical prototype of the SEA was designed. By using an incremental encoder the deflection over the spring is measured and used for calculations of the torque acting on the actuator. The controller implemented on the Single-Board RIO is capable of torque controlling the attached pendulum.
- **Simulation**: The structure of the SEA was implemented in MATLAB Simulink. First simulations were done by using a simple P-controller for the fixed pendulum. The transfer functions of the system were derived and then were used to calculate the bandwidth of the motor and the complete system. Later the model was verified by comparing results of experiments with the physical SEA prototype.
- **Control**: The before tested proportional controller was implemented on the Single-Board RIO. First torque control experiments with the P-controller have shown, that the free pendulum has problems performing the desired torque control task. By adding an integrating part this can be improved. The PI-controller was able to accurately torque control the pendulum. Three torque control tasks were implemented for demonstration reasons: gravity compensation, constant demand torque at the output and the virtual behavior of a spring can be simulated.

7.2 Conclusion

The goal of this thesis was to perform accurate torque control by using high-compliant SEA. To make the results visible, a SEA actuated pendulum should be able to perform different torque control tasks, such as zero torque at the output, gravity compensation or the behavior of a virtual spring.
If we only look at the actuator itself without any influence of the pendulum (output of the spring is fixed), the actuator can be controlled by using a simple P-controller. As soon as the influence of the pendulum is introduced, the proportional controller turned out to be too slow. Therefore, a new control structure has to be applied. A PI-controller is shown to be the better solution for torque control tasks of the free pendulum. A limiting factor in the performance turned out to be the capability of

the motor. Experiments have shown, that depending on the motor and the gear reduction, the system is not able to produce the demanded torques and corresponding speeds.

7.3 Outlook

The series elastic actuator developed in this paper, works for a one degree of freedom pendulum, if it is in contact with it surroundings. Since the idea behind this thesis is end-effector force control in legged locomotion, the next step would be to extend this work to two pendulums with two SEAs. The desired final result would be the implementation of a two-segment leg, both actuated with a SEA, on the quadruped robot. A combination of position control (during flight phase) and torque control (when interacting with its surrounding) should allow stable walking over unpredicted terrain of the quadruped robot.

Appendix A

NX Drawings

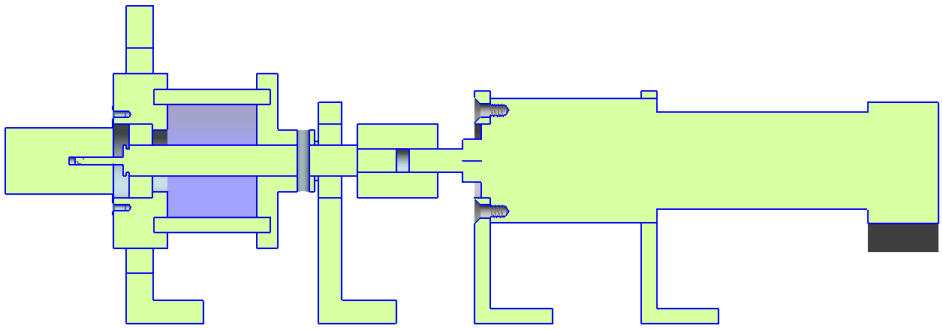

Figure A.1: Sideview of the assembly of the complete system: sensor, bottom and top part of the coupling, spring and motor with gearbox.

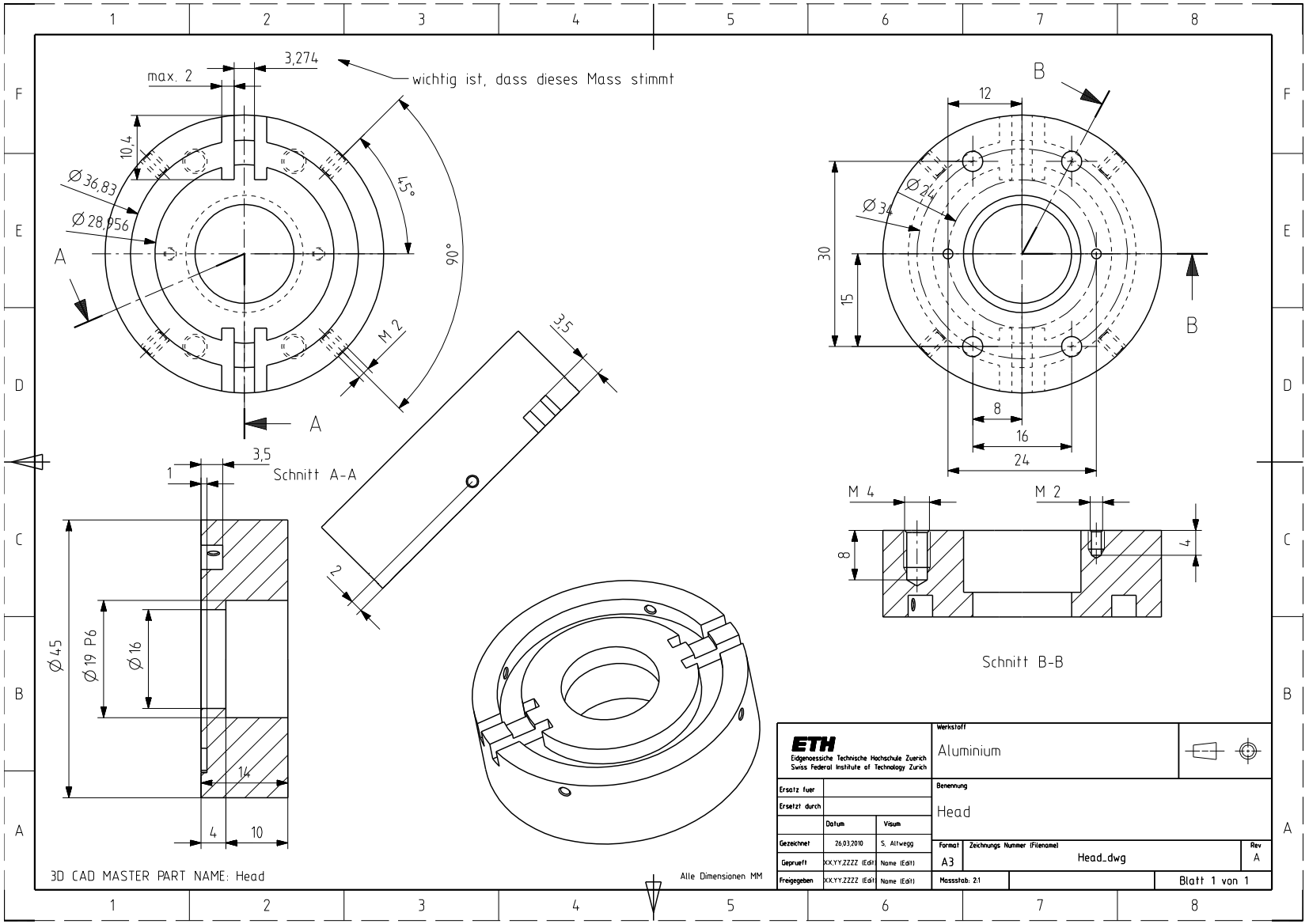
3,274
max. 2
wichtig ist, dass dieses Mass stimmt
10,4
Ø 36,83
Ø 28,956
45°
90°
A
M 2
3,5
2
Schnitt A-A
1
3,5
Ø 45
Ø 19 P6
Ø 16
14
4
10
B
12
Ø 24
Ø 34
30
15
8
16
24
M 4
M 2
8
4
Schnitt B-B
3D CAD MASTER PART NAME: Head
Alle Dimensionen MM
ETH
Eidgenoessische Technische Hochschule Zuerich
Swiss Federal Institute of Technology Zurich
Werkstoff
Aluminium
Benennung
Head
Ersatz fuer
Ersetzt durch
Datum
Visum
Gezeichnet
26.03.2010
S. Altwegg
Geprueft
XX.YY.ZZZZ (Edit)
Name (Edit)
Freigegeben
XX.YY.ZZZZ (Edit)
Name (Edit)
Format
A3
Zeichnungs Nummer (Filename)
Head_dwg
Rev
A
Massstab: 2:1
Blatt 1 von 1

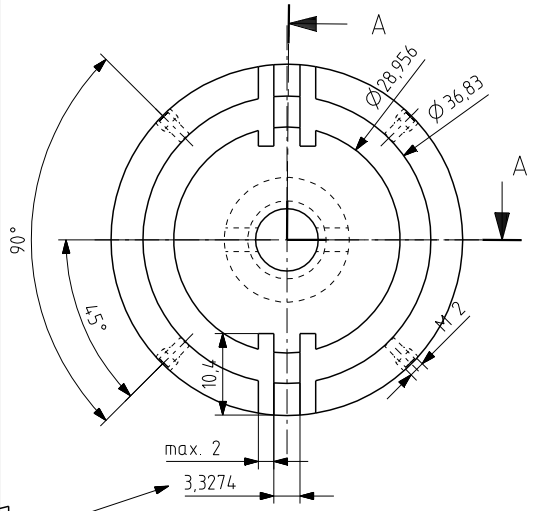

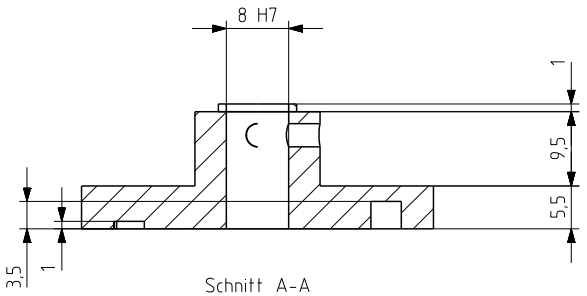

Schnitt A-A

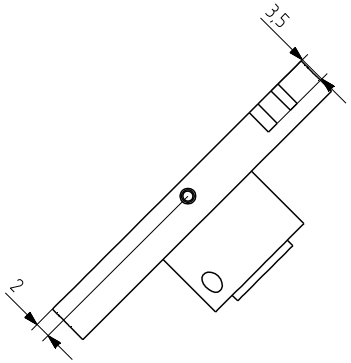

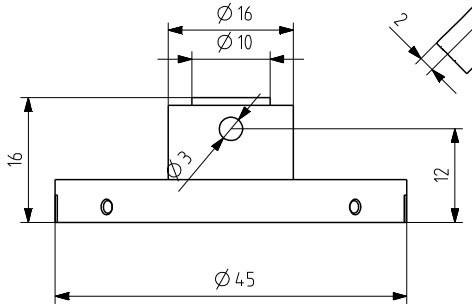

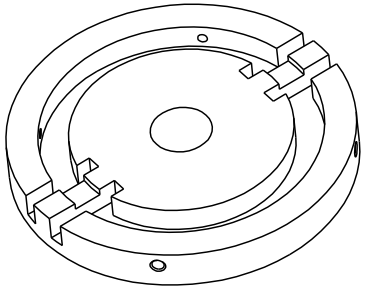

3D CAD MASTER PART NAME: Buttom

Alle Dimensionen MM

ETH Eidgenoessische Technische Hochschule Zuerich Swiss Federal Institute of Technology Zurich			Werkstoff: Aluminium		
Ersatz fuer			Benennung: Bottom		
Ersetzt durch					
	Datum	Visum			
Gezeichnet	26.03.2010	S. Altwegg	Format: A3	Zeichnungs Nummer (Filename): Bottom_dwg	Rev: A
Geprueft	XX.YY.ZZZZ (Edit)	Name (Edit)			
Freigegeben	XX.YY.ZZZZ (Edit)	Name (Edit)	Massstab: 2:1		Blatt 1 von 1

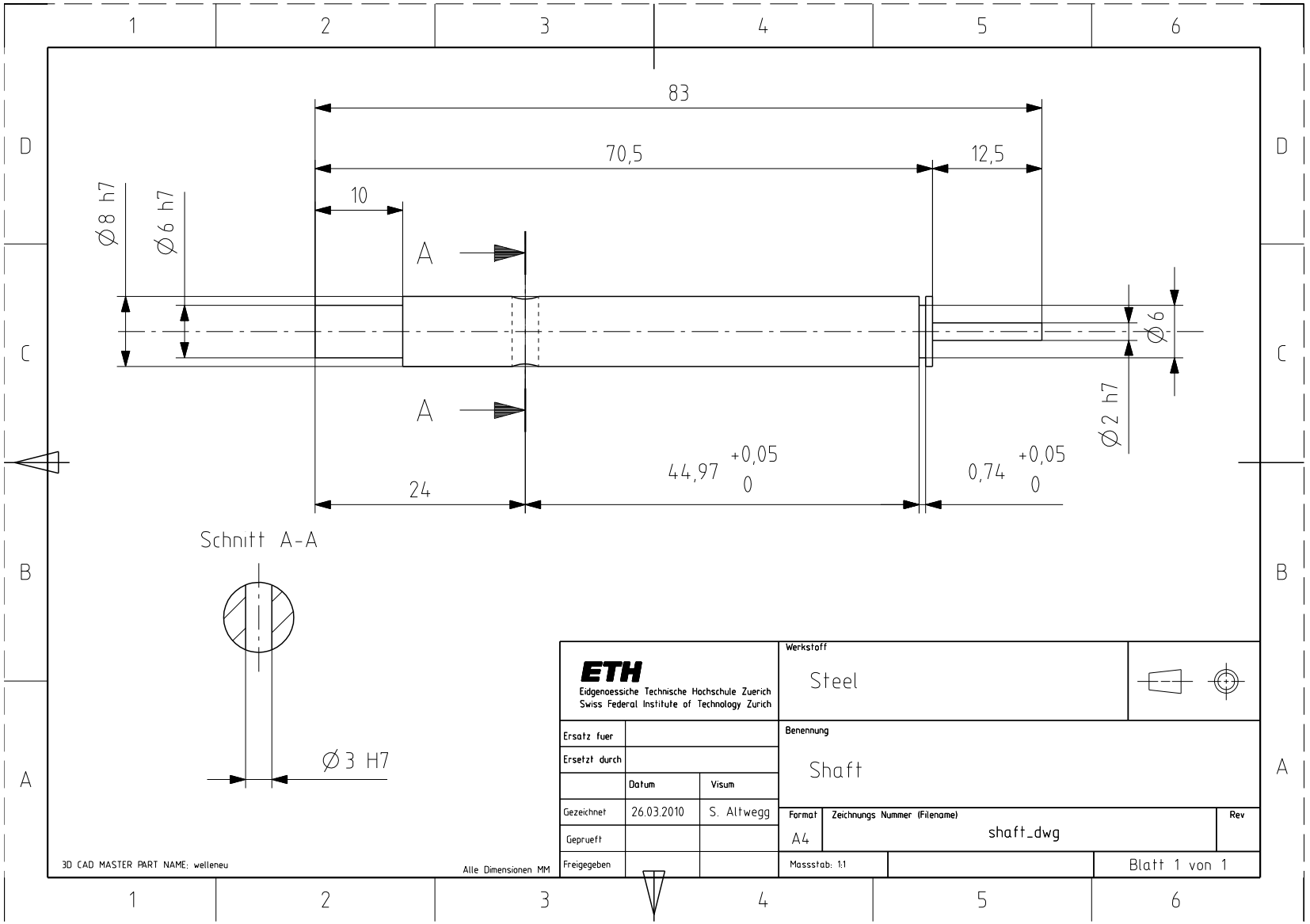
83
70,5
12,5
10
Ø8 h7
Ø6 h7
A
A
Ø6
Ø2 h7
44,97 +0,05 0
0,74 +0,05 0
24
Schnitt A-A
Ø3 H7
ETH
Eidgenoessische Technische Hochschule Zuerich
Swiss Federal Institute of Technology Zurich
Werkstoff
Steel
Benennung
Shaft
Ersatz fuer
Ersetzt durch
Datum
Visum
Gezeichnet
26.03.2010
S. Altwegg
Geprueft
Freigegeben
Format
A4
Zeichnungs Nummer (Filename)
shaft_dwg
Rev
Massstab: 1:1
Blatt 1 von 1
3D CAD MASTER PART NAME: welleneu
Alle Dimensionen MM

Appendix B

Data Sheets

B.1 Avago AEDA-3300 Series Incremental Kit Encoder

Table B.1: Avago AEDA-3300 TE1 Incremental Encoder Top-Down Version [6].

Characteristic	Value
CPR	20'000
CPR after decoding	80'000
Max frequency in kHz	650
Max. RPM	1950

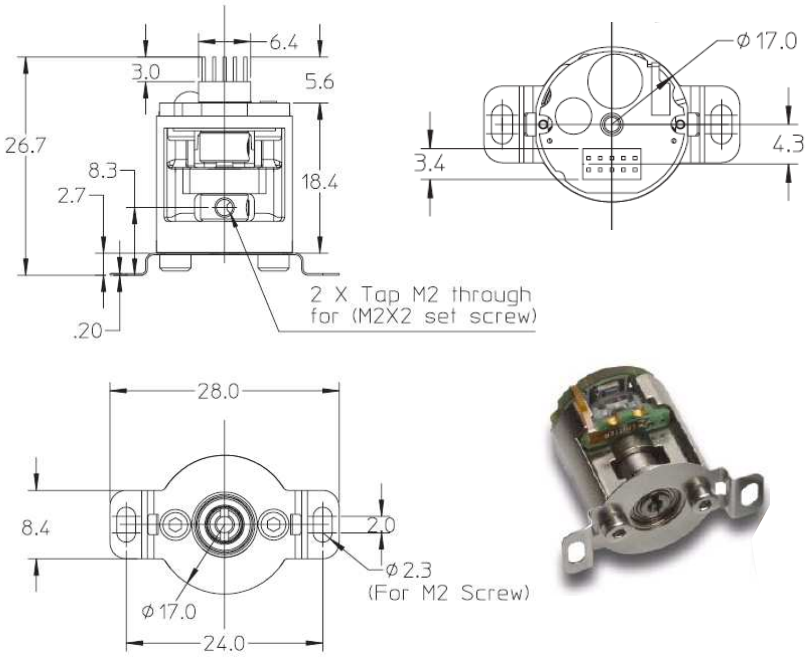

Figure B.1: Technical drawing of encoder, used for the sensor placement at the coupling of the spring, and a photo of the actual encoder.

B.2 Helical Torsional Spring

Table B.2: Helical Torsional Laser Cut Spring

	Unit	Value	Symbol
Spring constant	lbin at 90°	86.5 ± 8.7	
	Nm/rad	6.2223	k_s
Max. windup	°	±90	

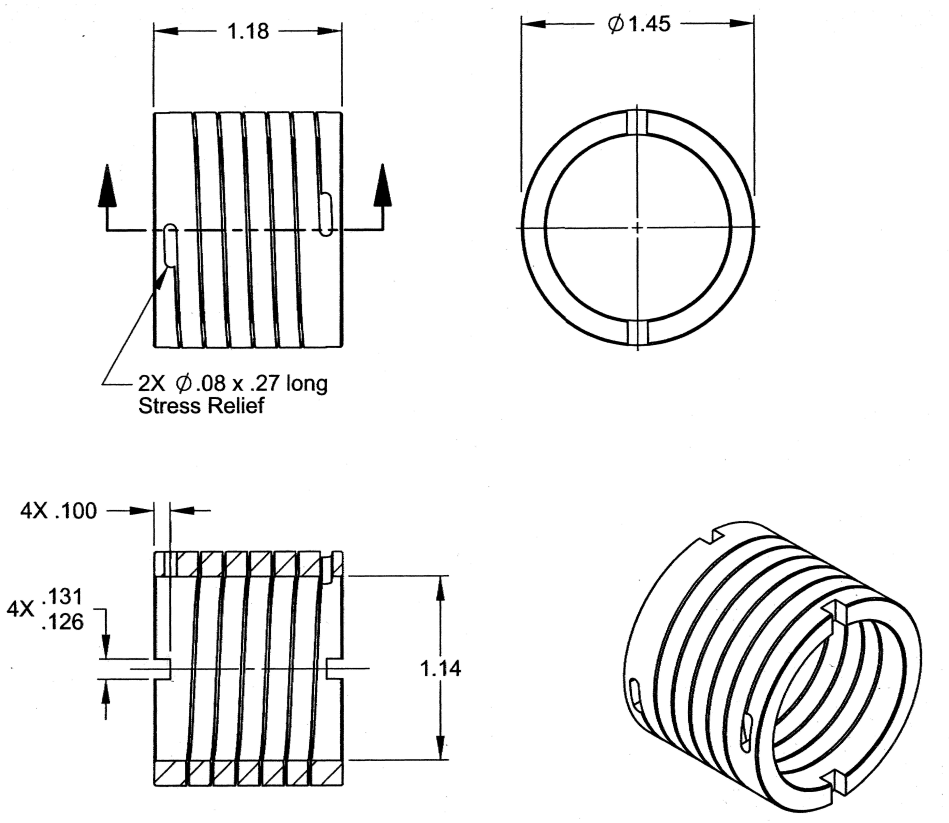

Figure B.2: Technical drawing of the spring used in this SEA, produces by Helical Products co., inc.

B.3 Maxon Motor RE 25 and Planetary Gearhead GP 32

Table B.3: Data sheet of Maxon motor components [5].

Characteristic	Unit	Value	Symbol
Maxon Motor RE 25 Ø25mm, Graphite Brushes, 20 Watt			
Article No.	-	339152	
Assigned Power Rating	W	20	
Nominal voltage	V	24	U
No load speed	min^{-1}	10900	
Stall torque	mNm	304	
Max. continuous torque	mNm	28.8	
Max. permissible speed	min^{-1}	14000	
Nominal current	A	1.42	
Max. efficiency	%	87.5	
Torque constant	Nm/A^{-1}	20.8	κ_i
Speed constant	$\text{min}^{-1}/\text{V}^{-1}$	460	κ_a
Rotor inertia	gcm^2	13.8	Θ_{mot}
Planetary Gearhead GP 32 C Ø32 mm, 1.0-6.0 Nm, Ceramic Version			
Article No.	-	166941	
Reduction	-	79:1	γ
Max.continuous torque	Nm	6	
Intermittently permissible torque at gear output	Nm	7.5	
Max. efficiency	%	70	η_{gb}
Mass inertia	gcm^2	0.7	Θ_{gb}
Combination Data			
Nominal voltage	V	24	U
No load speed	min^{-1}	138	
Max. continuous torque	mNm	6	
Stall Torque	mNm	7.5	

Appendix C

Function Derivations

C.1 Transfer Function of the Motor

As an input signal, the PID speed controller of the motor gets the desired velocity and the actual speed at the output of the motor in degrees. Therefore, φ_{mot} is multiplied by γ for the gearbox reduction and by $\frac{180}{\pi}$ to convert radiant to degree.

$$U(s) = (\dot{\Phi}_{des}(s) - \gamma \cdot \frac{180}{\pi} \cdot \dot{\Phi}_{mot}(s)) \cdot (k_p + s \cdot k_d + \frac{k_i}{s}) \tag{C.1}$$

The electrical circuit of the motor is simply the Laplace transform of the physical representation in equation (2.4).

$$I(s) = \frac{U(s) - \dot{\Phi}_{mot}(s) \cdot \kappa_i}{s \cdot L + R} \tag{C.2}$$

The torque that the actuator produced depends linearly on the motor current I. Additionally the output torque is reduced by the maximum efficiency of the gearbox η_{gb}. This leads to the torque acting on the mass of the motor and gearbox.

$$T_{mot}(s) = I(s) \cdot \kappa_a \cdot \eta_{gb} \tag{C.3}$$

With the torque from the spring acting on the motor, the Laplace transform of motion equation 2.3 is derived. The counteracting torque T_{spr} has to be reduced by the gear reduction γ because its effect on the mass is seen through the transmission.

$$\dot{\Phi}_{mot}(s) = \frac{T_{mot}(s) - \gamma \cdot T_{spr}(s)}{s \cdot \Theta_{tot}} \tag{C.4}$$

The open-loop transfer function of the motor ($L_{mot}(s)$) is the result of a combination of equations (C.1) - (C.4). The influence of the spring torque is neglected such that we get the transfer function of the motor without any load attached.

$$\frac{\dot{\Phi}_{mot}(s)}{\dot{\Phi}_{des}(s)} = L_{mot}(s) = \frac{\kappa_a \kappa_i \cdot (k_p + s \cdot k_d + \frac{k_i}{s})}{s \cdot \Theta_{tot} \cdot (s \cdot L + R) + \gamma \frac{180}{\pi} \kappa_a \eta_{gb} \cdot (k_p + s \cdot k_d + \frac{k_i}{s}) + \kappa_i \kappa_a \eta_{gb}} \tag{C.5}$$

C.2 Transfer Function of the Plant

The complete system gets as an input signal a desired velocity of the actuator $\dot{\varphi}_{des}$ and the output is the torque T_{spr} acting on the spring.
The Laplace transformed equation of the spring 2.1 results in:

$$T_{spr}(s) = \Phi_{mot}(s) \cdot \gamma \cdot (k_s + s \cdot d_s) \tag{C.6}$$

Then the Laplace transformed equation of the mass of the motor and the gearbox 2.3 is derived:

$$s^2 \cdot \Phi_{mot}(s) \cdot \Theta_{tot} = \eta_{gb} \cdot T_{mot}(s) - \gamma \cdot T_{spr}(s) \tag{C.7}$$

The combination of equation C.6 and C.7 leads to:

$$\frac{T_{spr}(s)}{T_{mot}(s)} = H_1(s) = \frac{\gamma \cdot \eta_{gb} \cdot (k_s + s \cdot d_s)}{s^2 \cdot \Theta_{tot} + \gamma^2 \cdot (k_s + s \cdot d_s)} \tag{C.8}$$

Now the equation for the DC-Motor 2.4, 2.5 is Laplace transformed:

$$T_{mot}(s) = \kappa_a \cdot I(s) = \frac{\kappa_a}{s \cdot L + R}(U(s) - s \cdot \Phi_{mot}(s) \cdot \kappa_i) \tag{C.9}$$

Replacing φ_{mot} in C.9 by taking C.6 results in:

$$T_{mot}(s) = \kappa_a \cdot I(s) = \frac{\kappa_a}{s \cdot L + R}(U(s) - s \cdot \frac{T_{spr}(s)}{\gamma \cdot (k_s + s \cdot d_s)} \cdot \kappa_i) \tag{C.10}$$

The equations C.8 and C.10 are now combined:

$$\frac{T_{spr}(s)}{U(s)} = H_2(s) = \frac{H_1(s) \cdot \kappa_a \cdot \gamma \cdot (k_s + s \cdot d_s)}{(s \cdot L + R) \cdot \gamma \cdot (k_s + s \cdot d_s) + H_1(s) \cdot s \cdot \kappa_a \cdot \kappa_i} \tag{C.11}$$

Then the equation C.1 of the EPOS motor controller is included, the input of the controller are velocities in [°/s]. Therefore we have:

$$U(s) = (k_p + s \cdot k_d + \frac{k_i}{s}) \cdot (\dot{\Phi}_{des}(s) - \frac{180}{\pi} \cdot \gamma \cdot s\Phi_{mot}(s)) \tag{C.12}$$

Again φ_{mot} is substituted in C.12 by taking C.6:

$$U(s) = (k_p + s \cdot k_d + \frac{k_i}{s}) \cdot (\dot{\Phi}_{des}(s) - \frac{180}{\pi} \cdot \frac{T_{spr}(s)}{(k_s + s \cdot d_s)}) \tag{C.13}$$

Reordering equation C.13 results in the open-loop transfer function of the plant P(s):

$$\frac{T_{spr}(s)}{\dot{\Phi}_{des}(s)} = P(s) = \frac{s \cdot k_p + s^2 \cdot k_d + k_i}{H_2^{-1}(s) + \frac{180}{\pi} \cdot \frac{s \cdot k_p + s^2 \cdot k_d + k_i}{k_s + s \cdot d_s}} \tag{C.14}$$

Appendix D

MATLAB Files

General Model, Model Analysis	Folder: /MATLAB/ModelAnalysis/..
init.m	initial values for the models and other m-files
show_pendel.m	function that visualized the pendulum behavior
TransferFunctions.m	calculations of all transfer functions
Plots.m	Bode and Nyquist plots of the transfer functions
ModelMotor.mdl	model of the motor loop
ModelPendFixed.mdl	model of the fixed pendulum
ModelPendFree.mdl	model of the free pendulum

Table D.1: MATLAB files belonging to Chapter 2 and 5: General Model and Model Analysis.

Model Identification	Folder: /MATLAB/ModelIdentification/..
Spring verification of the hopping leg	
Leg\DataAquisitionLeg.m	file for data acquisition of the hopping leg
Leg\DeflectionTest_xxxxxx_vxx.txt	files with the measured data of the hopping leg
Identification of the motor loop	
Motor\DataAquisitionMotor.m	file for data acquisition of the motor loop
Motor\Motor.mdl	model of the motor loop
Motor\init.m	file with the initial values for the motor model
Motor\MotorTest_xxxxxx_vxx.txt	files with the measured data of the motor
Identification of the spring in the SEA	
Spring\DataAquisitionSpring.m	file for data acquisition of the spring
Spring\SpringTest_xxxxxx_vxx.txt	files with the measured data of the spring
Identification of complete SEA	
System\DataAquisitionSystem.m	file for data acquisition of the complete system
System\System.mdl	model of the complete system
System\init.m	file with the initial values for the complete model
System\SysTest_xxxxxx_vxx.txt	files with the measured data of the system

Table D.2: MATLAB files belonging to Chapter 5: Model Verification.

Controller Implementation	Folder: /MATLAB/ControlModes/..
DataAquisitionModes.m	initial values for the models and other m-files
Gravity_xxxxxx_vxx.txt	files with measured data of the gravity compensation
Spring4_xxxxxx_vxx.txt	files with the measured data of spring behavior
ZeroTorque_xxxxxx_vxx.txt	files with the measured data of zero torque mode

Table D.3: MATLAB files belonging to Chapter 6: Controller Implementation.

Appendix E

NX Files

Physical SEA prototype	Folder: /NX/..
Head.prt	outer half of the spring coupling
Bottom.prt	inner half of the spring coupling
Shaft.prt	shaft that connects both halves
Assembly\assembly.prt	assembly of the complete system, including the actuator
Assembly\..	all the other files needed for the assembly

Table E.1: NX files of the coupling for the spring.

Appendix F

LabView Files

Controller Implementation	Folder: /LabView/..
invPend_sbRIO.lvproj	LabView project file
$FPGA\_InvPend\_inclForceSensor\_v01.vi$	VI for the torque control modes
$FPGA\_encoder\_v01.vi$	VI for the incremental encoder
$InvPend\_VelCTRL\_v01.vi$	VI for the different torque cont. modes
virt_pend.vi	sub VI for virtual spring torque cont.
torque_gravity.vi	sub VI for gravity compensation torque cont.

Table F.1: NX files of the coupling for the spring.

Bibliography

[1] M. Hutter: *Planar Hopping with a Robotic Leg*. Master's Thesis, ETH Zürich, 2009.

[2] Lino Guzzella: *Modeling and Analysis of Dynamic Systems*, ETH Zürich, Jul. 2009.

[3] Lino Guzzella: *Analysis and Synthesis of Single-Input Single-Output Control Systems*, vdf Hochschulverlag an der ETH Zürich, pp. 135-138, 2006.

[4] C. David Remy, Oliver Baur, Martin Latta, Andi Lauber, Marco Hutter, Mark Höpflinger, Céderic Pradalier, Roland Siegwart: *Walking and Crawling with ALOF - a Robot for Autonomous Locomotion on Four Legs*, Proceedings of the International Conference on Climbing and Walking Robots, Nagoya, Japan, 2010.

[5] http://www.maxonmotors.com: Maxon motor, gearbox and EPOS, June 2010.

[6] http://www.avagotech.com: Avago AEDA encoder, June 2010.

[7] Gordon Wyeth: *Control Issues for Velocity Sourced Series Elastic Actuators*. Proceedings of the Australasian Conference on Robotics & Automation 2006, Auckland, New Zealand

[8] http://www-clmc.usc.edu/Research/LearningLocomotion, June 2010

[9] D. Vischer, O. Khatib: *Design and Development of Torque-Controlled Joints*. Experimental Robotics vol. 1, pp. 271-286, 1990.

[10] D. Vischer, O. Khatib: *Design and Development of High-Performance Torque-Controlled Joints*. IEEE Trans. Robot Automat., vol. 11, pp. 537-544, Aug. 1995.

[11] A. Albu-Schäffer, S Haddadin, Ch. Ott, A. Stemmer, T. Wimböck, and G. Hirzinger: *The DLR lightweight robot: design and control concepts for robots in human environments*. Industrial Robot: An International Journal, vol. 34, no. 5, pp. 376-385, 2007.

[12] Marc H. Raibert: *Legged Robots*. Communications of the ACM, vol. 29 , no. 6, pp. 499 - 514, June 1986.

[13] J.E. Pratt, B.T. Krupp: *Series Elastic Actuators for legged robots*. Proceedings of SPIE - the international society for optical engineering, 2004.

[14] G.A. Pratt: *Low Impedance Walking Robots*. Integrative and Comparative Biology, vol. 42, pp. 174-181 ,2002.

[15] Gill A. Pratt, and Matthew M. Willamson: *Series Elastic Actuators.* IEEE International Conference on Intelligent Robots and Systems, vol. 1, pp. 399-406, 1995.

[16] Matthew M. Williamson: *Series Elastic Actuators.* M.S. thesis, Massachusetts Institute of Technology, June 1995.

[17] D.W. Robinson, J.E. Pratt, D.J. Paluska, and G.A. Pratt: *Series Elastic Actuator Development for a Biomimetic Walking Robot.* IEEE/ASME International Conference on Advanced Intelligent Mechatronics, Sept. 1999.

[18] David W. Robinson: *Design and Analysis of Series Ealasticity in Closed-loop Actuator Force Control.* PhD. thesis, Massachusetts Institute of Technology, June 2000.

[19] R. McN. Alexander: *Three Uses for Springs in Legged Locomotion.* The International Journal of Robotics Research, vol. 9, pp. 53-61,1990.